

Green and Facile Synthesis of Hybrid Composites with Ultralow Dielectric Properties from Water-Soluble Polyimide and Dual-Porous Silica Nanoparticles

Sunkyu Kim,[▽] Yeongje Lee,[▽] Jongmin Park, Yujin So, Hee-Tae Jung, Min Jae Ko, Jong Chan Won, Sunho Jeong,* and Yun Ho Kim*



Cite This: *ACS Appl. Mater. Interfaces* 2023, 15, 4408–4418



Read Online

ACCESS |

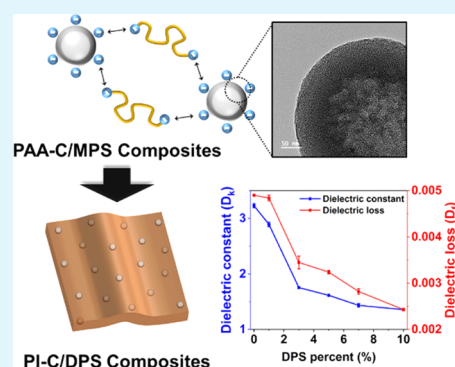
Metrics & More

Article Recommendations

Supporting Information

ABSTRACT: Here, we proposed an eco-friendly synthetic method for synthesizing hybrid composites with ultralow dielectric properties at high frequencies up to 28 GHz for true 5G communication from aqueous aromatic polyimide (PI) polymers and dual-porous silica nanoparticles (DPS). The “one-step” water-based emulsion template method was used to synthesize the macroporous silica nanoparticles (MPS). A substantially negative ζ potential was produced along the surface of MPS by the poly(vinylpyrrolidone)-based chemical functionalization, enabling excellent aqueous dispersion stability. The water-soluble poly(amic acid) (PAA), as a precursor to PI, was also “one-step” polymerized in an aqueous solution. The MPS were dispersed in a water-soluble PAA matrix to create the hybrid composite films using an entirely water-based approach. The compatibility between the PAA matrix and MPS was elucidated by investigating relatively diverse end-terminated PAAs (with either amine or carboxyl group). It was also discovered that, during a thermally activated imidization reaction, the MPS are in situ converted into the DPS with macro- and microporous structures (with a surface area of 1522.4 m²/g). The thermal, dielectric, mechanical, and morphological characteristics of each composite film were examined, while the amount of DPS in the PI matrix varied from 1 to 20 wt %. With the addition of 5 wt % DPS as an optimum condition, it showed ultralow dielectric properties, with the D_k and D_f being 1.615 and 0.003 at a frequency of 28 GHz, respectively, and compatible mechanical properties, with the tensile strength and elastic modulus being 78.2 MPa and 0.32 GPa, respectively. These results can comprehensively satisfy various physical properties required as a substrate material for 5G communication devices.

KEYWORDS: polyimide, dual-porous, silica, composite, low dielectric



1. INTRODUCTION

Low dielectric materials that can reduce the transmission loss of communication elements are becoming increasingly popular with the advent of the 5G communication era.^{1,2} For high-speed communication, there is a demand in particular for polymers and polymer–inorganic composite materials with a low dielectric constant (D_k) of 2.8 or less and a low dielectric loss (D_f) of 0.004 or less even at frequencies of 10 GHz or more.^{3,4} Polyimide (PI) polymers have been widely used as a substrate material for printed circuit boards (PCBs) because of their high-temperature durability, excellent mechanical property, and excellent chemical stability.^{5–7} However, typical aromatic PIs have been considered unsuitable for interlayer dielectric applications for 5G communication since they have D_k values between 3.1 and 3.5 and D_f values of over 0.005.

Several studies have been reported to have reduced the dielectric properties of PI polymers while maintaining superior physical properties.^{8,9} First, it has been proposed that the fluorinated and aliphatic-modified PIs can reduce polarization and introduce free volume.^{10,11} Han et al. decreased the

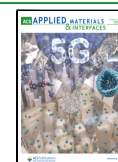
dielectric constant to 2.78 at 1 MHz by introducing a hyperbranched fluorine unit into the main PI chain with a cross-linking agent.¹² Feng et al. incorporated two-dimensional fluoro-graphene sheets into PI composites to decrease the dielectric constant to 2.09 at 1 MHz.¹³ However, when chemically changing the molecular structure of PIs, insufficient thermal and mechanical stability remains a critical challenge to be overcome.

Therefore, research is underway toward introducing air voids ($D_k = 1$) directly into the conventional aromatic PI matrixes with excellent physical properties. Various methods of introducing porous structures have been reported, such as manufacturing a PI aerogel,¹⁴ making a porous PI film using a

Received: September 8, 2022

Accepted: December 2, 2022

Published: December 15, 2022



sacrificial template,¹⁵ and preparing a porous structure using the in situ balloon method.¹⁶ Among them, research on introducing hollow silica particles (HSPs) is drawing attention because it can maintain the mechanical properties of the final PI composites well and effectively control the pore structure.¹⁷ Ha et al. incorporated 5 wt % of hollow microspheres with a diameter of 1.5 μm and reduced the dielectric constants of the aromatic PI from 3.1 to 1.81 at 1 kHz.¹⁸ Jin's group reported that the dielectric constant could be lowered to 2.09 at 1 kHz by introducing surface-functionalized HSPs into the aromatic PI matrix at 10 wt %.¹⁹

However, in previous studies of manufacturing PI/HSP composite films, it was discovered that a process of removing polymer nanoparticles used as a template for HSP preparation is inevitably required. This is then followed by an additional surface treatment process to improve dispersibility with the poly(amic acid) (PAA) as a precursor of PI.²⁰ Additionally, most studies have only used a single macroporous structure at the center of the HSP to introduce air voids. In addition, the PI/HSP composite films have been prepared with highly toxic and difficult-to-handle solvents like *N*-methyl-2-pyrrolidone. Dimethylformamide or dimethylacetamide is a typical solvent for preparing PAA solutions. As environmental concerns become increasingly important in the electronics industry, efforts to reduce the use of such toxic solvents are strongly required.²¹ In addition, although it is necessary to develop low dielectric materials for a high-frequency region of 28 GHz or higher to apply it to a true 5G communication device, most studies mainly deal with the D_k reduction effect in the frequency region of 1 kHz to 1 GHz. And it is known that the transmission loss of actual 5G communication devices using a high frequency of 10 GHz or higher is greatly affected by the D_f characteristic rather than the D_k of the material.^{3,4} Nevertheless, the experimental results on the D_f characteristics are insufficient compared to those of the D_k reduction technique.

In this work, we proposed an eco-friendly synthetic method for synthesizing hybrid composites with ultralow dielectric properties at high frequencies up to 28 GHz for true 5G communication from aqueous aromatic polyimide (PI) polymers and dual-porous silica nanoparticles (DPS). The "one-step" water-based emulsion template method was used to synthesize macroporous silica nanoparticles (MPS). Through a surface functionalization by the poly(vinylpyrrolidone), a highly negative ζ potential was established along the surface of MPS, enabling excellent dispersion stability in the aqueous mixture. In an aqueous solution, water-soluble PAAs as a precursor for the PI polymers were also "one-step" polymerized. The hybrid composite films were prepared by an all-water-based "green" process of dispersing the MPS in a water-soluble PAA matrix. The compatibility between the PAA matrix and MPS was elucidated by investigating differently end-terminated PAAs with either amine or carboxyl groups. The chemical structures of amine- and carboxyl-terminated PAAs, denoted as PAA-A or PAA-C, were characterized by ¹H-NMR (nuclear magnetic resonance) spectroscopy. Through thermal imidization reactions, they underwent cyclodehydration to become PI-A and PI-C. Interestingly, it was discovered that the MPS, with a surface area of 26.9 m²/g, are converted into the DPS comprising macro- and microporous structures, with a surface area of 1522.4 m²/g, during a thermally activated imidization reaction. By varying the loading of DPS as a filler in the range of 1–20 wt %, the surface morphology and dielectric

properties of the PI-A/DPS or PI-C/DPS composites were systematically investigated. The D_k and D_f decreased significantly down to ultralow values of 1.783 and 0.003 and 1.615 and 0.003 at frequencies of 10 and 28 GHz, respectively, with the addition of 5 wt % DPS into the PI-C matrix as an optimum condition, evidently attributable to characteristic hierarchical air voids spatially distributed inside the DPS.

2. EXPERIMENTAL SECTION

2.1. Materials. 3,3',4,4'-Biphenyltetracarboxylic dianhydride (BPDA) and *p*-phenylenediamine (PDA) were purchased from Sunlight Chem., China, and used after drying at 250 and 80 °C, respectively. Tetraethyl orthosilicate (TEOS), ammonium hydroxide solution (NH₄OH, 28.0–33.0% NH₃ basis), 1,2-dimethylimidazole (DMIZ), hexadecyltrimethylammonium bromide (CTAB), and poly(vinylpyrrolidone) (PVP, 55,000 g/mol) were purchased from Sigma-Aldrich and used as received.

2.2. Synthesis of Macroporous Silica Nanoparticles. An emulsion template method was used to synthesize the MPS. A mixture of 25.3 g of DI water, 12.9 g of ethyl alcohol, and 0.08 g of CTAB was stirred for 5 min. After stirring for 5 min, 0.47 g of TEOS was added to the mixture and stirred for 10 min. Then, 0.45 g of NH₄OH was added as a basic catalyst. In the case of functionalizing the surface of silica nanoparticles, 25 mg of PVP was added with an additional NH₄OH catalyst. The reaction solution was stirred for 3 h to complete the chemical reactions. The resulting nanoparticles were collected and washed by a centrifugation method. As a control experiment, we have also synthesized the dense silica nanoparticles. A mixture of 37.6 g of TEOS, 37.6 g of DI water, and 221.8 g of ethyl alcohol was stirred, the reaction solution was heated to 50 °C, and NH₄OH was added as a basic catalyst. After completing the chemical reactions for 2 h, the reaction solution cooled down to room temperature. The resulting nanoparticles were collected and washed by a centrifugation method. All synthesis procedures were carried out in air.

2.3. Synthesis of End-Terminated PAAs as Water-Soluble Precursors. Following our previous studies, the BPDA/PDA-based PAA-A or PAA-C were prepared using a one-step polymerization process in an aqueous solution with 1,2-dimethylimidazole (DMIZ), which enables the formation of an ammonium salt with the carboxylate group of PAA.^{22,23} It was synthesized in a three-neck flask equipped with a mechanical stirrer under a nitrogen atmosphere. By a 0.01 molar ratio over the equimolar condition, dianhydride (BPDA) and diamine (PDA) monomers were used in a slightly excess amount to terminate the end group with the desired charge. For instance, DMIZ (200 mmol) and PDA (80 mmol) were added to DI water (463 mL) to polymerize PAA-C, and then, the mixture was stirred at 25 °C for 1 h. After the mixture dissolved, BPDA (80.8 mmol) was added, and the mixture was stirred at 70 °C for 18 h to obtain a viscous 10 wt % PAA-C aqueous solution.

2.4. Preparation of PI/DPS Hybrid Composite Films. The PI/DPS composite films were prepared by simple mixing and solution casting. First, the MPS were dispersed in DI water by ultrasonic treatment. The aqueous MPS dispersion was then added to the PAA solution to the desired content in the range of 1–20 wt % relative to the PAA solid content. The solutions were vigorously mixed for 30 min at 2000 rpm using a revolutionary mixer (ARE-310, THINKY). Each mixing solution of PAA-A (or -C)/MPS was cast onto the glass substrates to a thickness of 1000 μm . The PAA-A (or -C)/MPS films were thermally dried at 40 °C for 1 h in a vacuum oven (HERAEUS vacuum oven, Thermo Scientific). The dried films were imidized for 40 min at various step curing temperatures of 50, 80, 100, 150, 200, 250, 300, and 350 °C, respectively. During this thermal imidization process, the MPS are converted to DPS with a hierarchically dual-porous structure. Finally, the PI-A (or -C)/DPS-# composite films with a thickness of $\sim 30 \mu\text{m}$ were obtained, where # denotes the wt % content of DPS.

2.5. Characterization. A scanning electron microscope (SEM, Merlin FE-SEM, ZEISS) and a transmission electron microscope

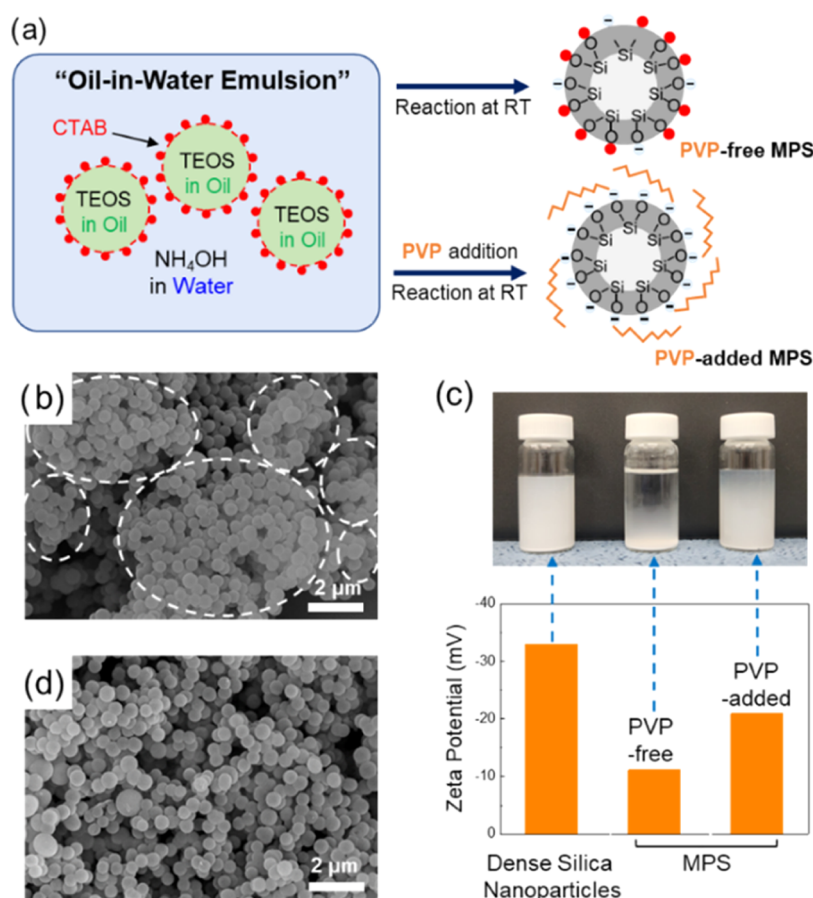


Figure 1. Schematic representation for the synthetic procedures of (a) PVP-free and PVP-added MPS via heterogeneous nucleation/growth reactions based on the oil-in-water emulsion templating method. (b) SEM image of PVP-free MPS. (c) Optical image and ζ potential of aqueous solutions containing dense silica nanoparticles, PVP-free MPS, and PVP-added MPS 3 days after sonication. (d) SEM image of PVP-added MPS.

(TEM, Tecnai G2 F30 S-Twin, FEI) were used to examine the morphologies of silica nanoparticles. The ζ potential of silica nanoparticles was analyzed with a ζ -potential analyzer (ELS-Z, Otsuka). A residual solvent signal was used as an internal standard to obtain the ^1H nuclear magnetic resonance (^1H -NMR) spectra using a Bruker advance 400 MHz spectrometer (Billerica, MA). Size exclusion chromatography (SEC) was conducted in *N*-methyl-2-pyrrolidinone (NMP) solution with 0.02 M H_3PO_4 and 0.02 M LiBr at 50 $^\circ\text{C}$ with a flow rate of 0.8 mL/min on the Shodex (Showa Denko, Minato, Japan). The instrument was equipped with three poly(hydroxy methacrylate) columns (multipore) with a molar mass of 200–20,000,000 g/mol. Fourier transform infrared (FT-IR) spectra were obtained using a Bruker α -P spectrophotometer in the range of 650–4000 cm^{-1} under ambient conditions. The dielectric properties of composite films were measured using an Agilent E5080B network analyzer (Keysight) equipped with a TE mode cavity resonator for frequencies of 10 and 28 GHz (AET, Japan). The surface morphology and roughness of PI/DPS composite films were analyzed using a SEM and a 3D laser confocal microscope (LCM, VK-X200, Keyence, Japan). At room temperature, the tensile properties of the composite films were measured using a universal testing machine (UTM, ST-1000, SALT, Korea) with a strain rate of 1.0 mm/min. The reported values of each sample with the dimension of 10 mm \times 50 mm \times 50 μm (width \times length \times thickness) were averaged for five specimens in each case according to the ASTM D882 standard.

3. RESULTS AND DISCUSSION

3.1. Synthesis of Macroporous Silica Nanoparticles with a Highly Negative ζ Potential. TEOS is a chemical precursor used in a sol–gel reaction to synthesize silica

nanoparticles.^{24–26} The dielectric properties of inorganic materials attribute to polarization behaviors at given frequency conditions, which are predominantly determined by the composition of them. Among a variety of binary oxides, silica materials have low electronic polarization contributions at high-frequency regimes. Thus, they have been recognized as an appropriate candidate inorganic material that can exhibit low dielectric properties in inorganic–organic hybrid composites.^{17–19} The TEOS precursor has four alkoxy groups undergoing consecutive hydrolysis and condensation reactions to form the metal oxide skeletons. We have designed the TEOS precursors' heterogeneous nucleation/growth reaction for the "one-step" MPS synthesis (Figure 1a). The CTAB was added as a cationic surfactant to the mixture of ethyl alcohol, TEOS, and DI water to form the oil-in-water emulsions. The ethyl alcohol and DI water act as oil and water phases, respectively. The TEOS is immiscible with DI water but miscible with ethyl alcohol. Thus, by agitating the mixture (comprising the ethyl alcohol, TEOS, DI water, and CTAB), the submicron-sized oil droplets, composed of TEOS and ethyl alcohol, are dispersed in a water matrix phase. Ionized cationic surfactants stabilize the surface of oil phases. Adding NH_4OH as a basic catalyst triggers sol–gel reactions of TEOS precursors confined inside the oil droplets. The NH_4OH distributed in the water undergoes an inward diffusion inside the oil droplets. This activates TEOS precursor's chemical reactions at the interface between the water and oil phases, enabling a heterogeneous nucleation reaction. The nuclei grow

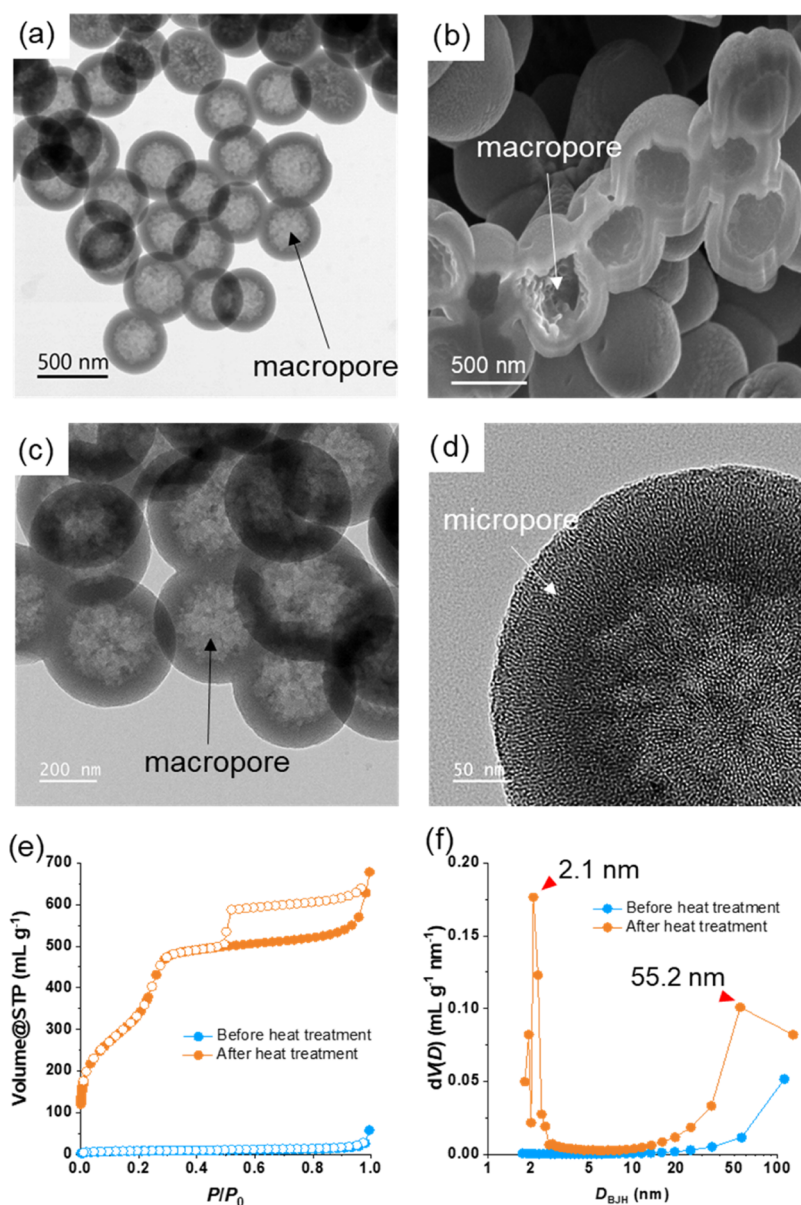


Figure 2. (a) TEM image and (b) cross-sectional FIB-SEM image of MPS. (c) TEM image and (d) high-resolution TEM image of heat-treated MPS. (e) Nitrogen adsorption isotherms. Filled circle: adsorption branch; Opened circle: desorption branch. (f) Pore size distribution (estimated from the adsorption branch by BJH analysis) of MPS according to heat treatment.

gradually by successive inward diffusion of the basic catalyst from the outer water phase and outward diffusion of TEOS precursors from the inner oil phase. Such localized growth reactions at the heterogeneous interfaces lead to the formation of MPS. An activation of heterogeneous nucleation/growth reactions supports that an emulsion-based sol–gel reaction was accomplished at room temperature.

Unfortunately, the ζ potential of MPS reduces because of the growth reaction at the interface that includes the cationic surfactant. The Si–O[−] groups present on the surface of MPS become neutralized by cationic surfactants, which significantly diminishes an electrostatic repulsive force. It is observed that as-synthesized MPS are highly aggregated into large particle assemblies (Figure 1b). Figure 1c shows that, although the dense silica nanoparticles have a ζ potential as high as −33.0 mV, the as-synthesized MPS have a ζ potential as low as −11.1 mV. As a control experiment, we synthesized the dense silica

nanoparticles by reacting TEOS precursors with DI water and NH₄OH (without a surfactant) at an elevated temperature of 50 °C (Figure S1a). The pH of the reaction solution was set to 11. The nuclei formed in a homogeneous reaction solution are grown gradually into dense silica nanoparticles. The surface of silica particles is composed of silanol groups (Si–OH). Under basic aqueous surroundings, they are spontaneously transformed into negatively charged Si–O[−] groups by a deprotonation reaction. This enables the development of a highly strengthened repulsive force between neighboring particles and prevents interparticular coagulation during synthetic reactions. As shown in Figure S1b, the dense silica nanoparticles are spherical and free of undesirable agglomerations.

The highly porous silica particles should be well dispersed in a polymeric matrix to facilitate the hybrid composites with ultralow dielectric properties. We incorporated poly-

(vinylpyrrolidone) (PVP) as a surface modifier, while the sol-gel reactions of the TEOS precursor proceed at the heterogeneous interface to resolve this critical issue (Figure 1a). The lone pairs present in pyrrolidone rings of PVP monomer units undergo a physical interaction with negatively charged ions.²⁷ It is presumed that the Si-O⁻ groups are anchored by the pyrrolidone rings of PVP polymers and become free from the hexadecyltrimethylammonium cations. All Si-O⁻ groups are not captured due to a steric hindrance of PVP polymers, so some Si-O⁻ groups can be exposed to outer surroundings. The ζ potential of PVP-added MPS was measured to be as high as -20.9 mV, comparable to the value of dense silica nanoparticles, as shown in Figure 1c. The distinctively different dispersion stability of PVP-free and PVP-added MPS is confirmed in the images and UV-visible spectra of aqueous suspensions for both particles, as shown in Figures 1c and S2. According to the SEM image in Figure 1d, it is shown that the PVP-added MPS are free of agglomerations and dispersed well without forming aggregates. In this study, the PVP-added MPS were used as an inorganic nanofiller for formulating the aqueous mixture for hybrid composite films.

3.2. In Situ Conversion of Macroporous Silica Nanoparticles into Dual-Porous Silica Nanoparticles.

Figure 2a,b shows TEM and focused ion beam combined scanning microscopy (FIB-SEM) images of MPS. It is observed that the internal pores, with an average diameter of 300 nm, are surrounded by the dense silica shell layer. As seen in TEM images in Figure 2c,d, the heat-treated MPS comprise internal macropores and outer micropores inside the shell layer. We thermally annealed the MPS at 350 °C, identical to the thermal imidization reaction of the PI matrix.

The nitrogen adsorption analysis was used to describe the microporous MPS structures before and after heat treatment (Figure 2e,f). The MPS before heat treatment are slightly porous with a surface area as low as 26.9 m²/g due to an internal macropore and outer dense shell layer. The MPS after heat treatment display obvious isotherms that suggest the presence of two separate porous structures, whereas the MPS before heat treatment exhibited a small amount of N₂ adsorbed (Figure 2e). The rapid increases at low relative pressure, followed by the moderate increase close to a relative pressure of 1 indicate the presence of micro- and macroporous structures. The pore diameter was estimated by the Barrett-Joyner-Halenda (BJH) analysis²⁸ at 2.1 and 55.2 nm, respectively (Figure 2f). After heat treatment, the pore volume of MPS was measured to be 0.95 mL/g with a large Brunauer-Emmett-Teller surface area (S_{BET}) of 1522.4 m²/g.

We performed a spectroscopic analysis to investigate a chemical evolution in the MPS during the heat treatment (Figure S3). Figure S3a shows the X-ray photoelectron spectroscopy (XPS) Si 2p spectrum of as-synthesized MPS. The spectrum was deconvoluted into peaks positioned at binding energies of 103.2 and 102.2 eV, stemming from the silicon in siloxane (Si-O-Si) bonds and the silicon with an alkoxy or hydroxyl group (Si-O-C or Si-O-H), respectively.²⁹ The atomic fraction of silicon with the alkoxy/hydroxyl group was calculated to be 37.9% based on a semiquantitative study using an areal integration of each peak. This indicates that a part of TEOS precursors does not take part in successive sol-gel reactions. The siloxane skeletons formed by a partial condensation reaction construct a particular macroporous morphology. It can be expected that the remnant sol-gel reactions are thermally activated further,

enabling the formation of more strengthened siloxane skeletons. The single symmetric peak became prominent at a binding energy of 103.2 eV with the extinction of the peak at a binding energy of 102.2 eV as shown in the Si 2p XPS spectrum for MPS after thermal treatment (Figure S3b). This suggests that sol-gel reactions are finished consuming all alkoxy/hydroxyl groups of TEOS precursors. The thermal decomposition is also confirmed by the fact that, in the FT-IR spectroscopy spectrum, any kind of peaks other than siloxane bonds were annihilated after thermal annealing (Figure S4).^{30,31} According to the thermogravimetric analysis data in air for MPS (Figure S5), the weight loss approaches the value of 34.3 wt %. This is attributed to the evaporation of alcohol and water molecules by further sol-gel reactions and the thermal decomposition of CTAB organic molecules and PVP polymers. Thus, it can be speculated that while thermal annealing proceeds, a huge amount of byproducts and organic/polymeric residues are vaporized, and the preformed siloxane skeletons sustain the internal vapor pressure, not collapsing the morphological structure of MPS. Notably, this results in the formation of micropores inside the outer shell layer. In this study, the thermally treated MPS with internal macropores and outer micropores are denoted as dual-porous silica nanoparticles (DPS).

The prerequisites as inorganic fillers for facilitating hybrid composites with low dielectric properties are as follows: (i) absence of agglomerated particle assemblies, (ii) chemical compatibility with a polymeric matrix, (iii) presence of a large number of air voids (pores), and (iv) absence of functional groups with electric dipoles. The first two prerequisites are paramount in mixing with the water-soluble PAA precursors. Those are satisfied by the characteristic surface properties of MPS, as discussed in the previous section. The other two prerequisites should be satisfied by the morphological and chemical properties of DPS distributed inside the PI matrix. Note that the DPS have a surface area as high as 1522.4 m²/g under the presence of macro/micropores. The alkoxy/hydroxyl groups of TEOS precursors and the polar groups included in the CTAB organic molecules and the PVP polymers can deteriorate the dielectric properties of composite films. For the case of the DPS developed in this study, such impurities were removed completely by a thermal imidization process. Thus, we believe that the DPS provide a strong advantage as the inorganic filler for facilitating low dielectric properties.

3.3. Synthesis of Water-Soluble Amine/Carboxyl-Terminated PAA Precursors. Uniform dispersion of nanofillers with low dielectric properties in a polymer matrix is of paramount importance in manufacturing low dielectric polymer composite films. The dispersion of the nanofillers is strongly influenced by the electrical and chemical environment of the dispersion medium when the nanofillers are hybridized with the polymer matrix, such as polymer matrixes and solvents.³² In this study, to confirm the compatibility of MPS with a highly negative ζ potential of more than -20 mV in the PAA matrix, water-soluble BPDA-pPDA-based PAAs having positive or negative charges at the end groups were prepared. As shown in the molecular structure of Figure S6a, PAA-A and PAA-C were eco-friendly polymerization in water as a solvent as following our previous studies.^{22,23} When PAA-A and PAA-C are solubilized in water, the -NH₂ group has a positive charge in the -NH₃⁺ state, and the -COOH group has a negative charge in the -COO⁻ state. Since the characteristic -COOH group of PAA in the main chain forms ammonium

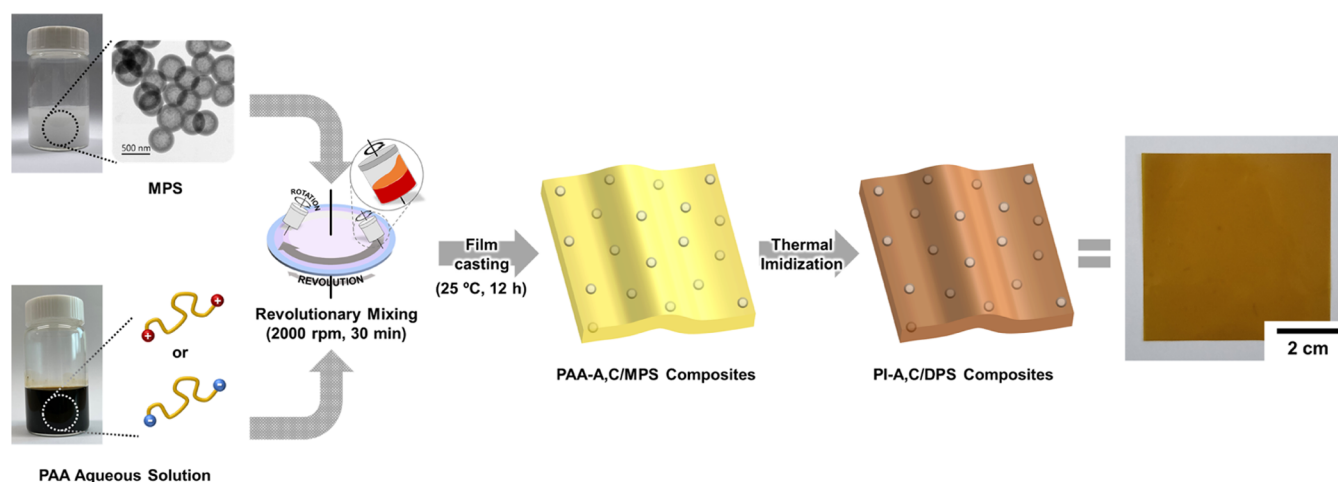


Figure 3. Schematic representation for the preparation of PI/DSP composite films based on an aqueous process using two end-terminated PAAs and PVP-added MPS.

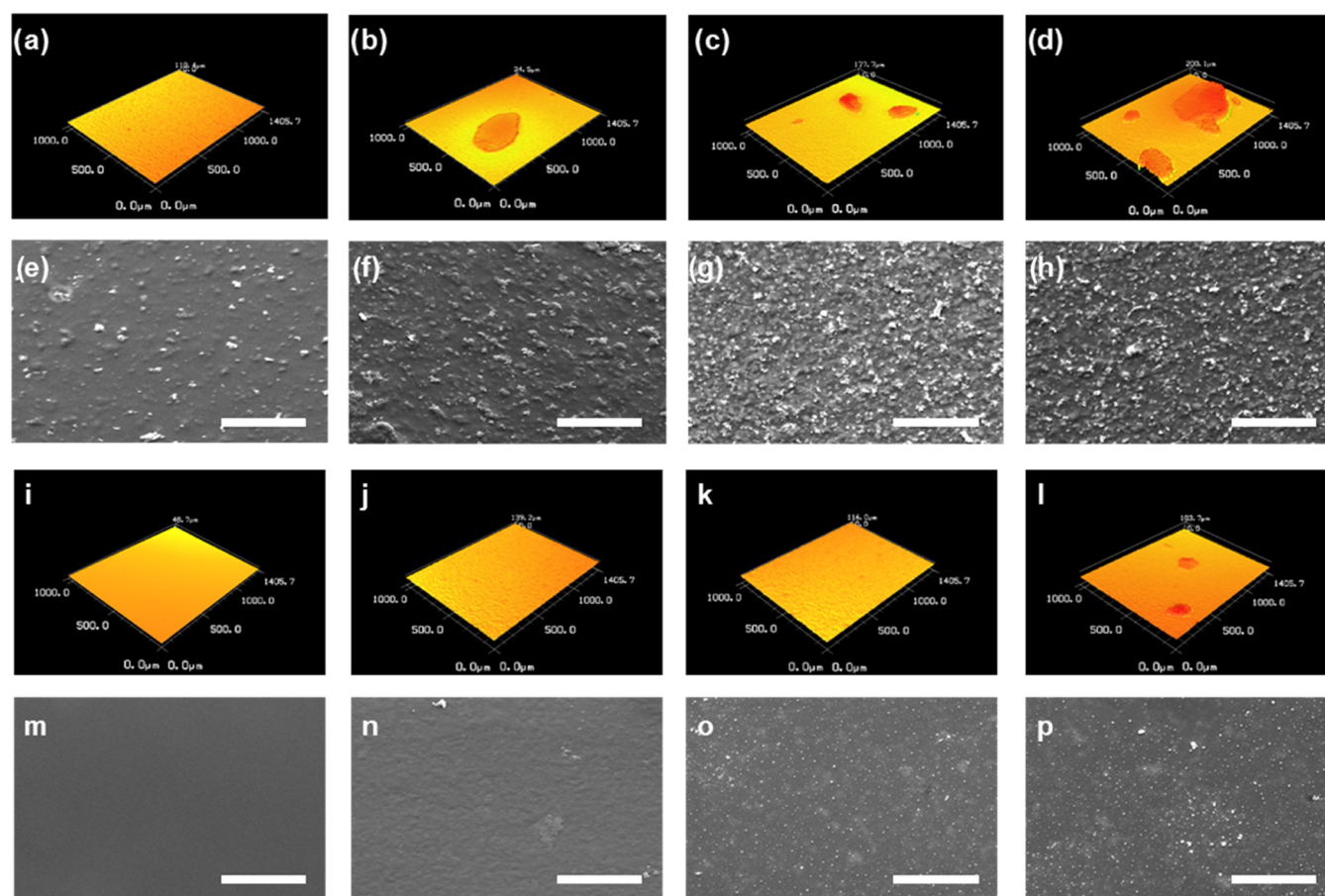


Figure 4. LCM and SEM images of PI-A/DPS and PI-C/DPS composite films at different DPS contents. (a, e) PI-A/DPS-1, (b, f) PI-A/DPS-5, (c, g) PI-A/DPS-7, and (d, h) PI-A/DPS-10. (i, m) PI-C/DPS-1, (j, n) PI-C/DPS-5, (k, o) PI-C/DPS-7, and (l, p) PI-C/DPS-10. All scales of SEM images are 100 μm .

salt foam with DMIZ,³³ the state of charge in each PAA is determined by the type of end-terminated group.

The chemical structures of PAA-A and PAA-C were analyzed by ^1H -NMR, as shown in Figure S6b. In both PAA-A and PAA-C, the hydrogen of the aromatic ring can be observed at 7.3–8.3 ppm, and hydrogen derived from the amide group can be observed at 10.7–11.2 ppm. Nitrogen in DMIZ makes a salt form via an acid–base reaction with the

–COOH group of the PAA backbone, representing peaks at 2.3, 3.3, 6.8, and 7.1 ppm. Generally, the end groups of PAA are equivalent to –NH₂ and –COOH groups. The end groups of PAA-A and PAA-C used in this study were intentionally designed to have predominantly either –NH₂ or –COOH groups, respectively. As shown in Figure S6b, characteristic peaks of –NH₂ or –COOH groups can be confirmed at 6.67 and 8.73 ppm, respectively, and the relative ratio of end groups

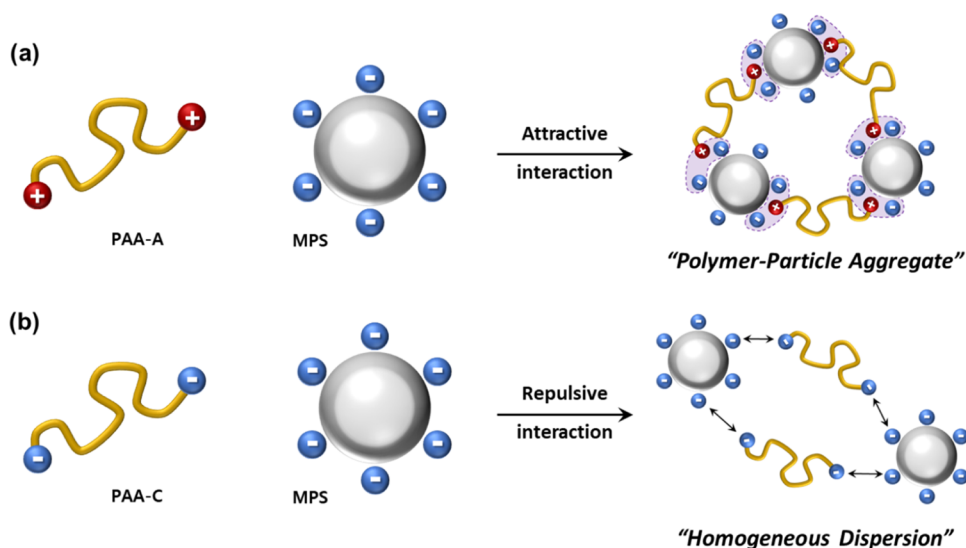


Figure 5. Schematic representation of the dispersion stability of MPS in differently end-terminated (a) PAA-A and (b) PAA-C as matrices.

can be confirmed through the integral area of each characteristic peak. In the case of PAA-A, it can be seen that 80.7% of $-\text{NH}_2$ and 19.3% of $-\text{COOH}$ form end groups, and PAA-C has end groups of 28.1% of $-\text{NH}_2$ and 72.0% of $-\text{COOH}$. Although it is not possible to completely control the end group with a single species, it is sufficient to control the dispersibility of MPS. The weight-averaged molecular weight (M_w) of the PAA-A and PAA-C obtained from SEC was 29.3 and 28.4 kg/mol, respectively, and their dispersity (\bar{D}) was measured to be 2.64 and 2.61, respectively (Figure S7). In particular, for solely investigating a critical effect of the PAA precursors' end group, the PAA-A and PAA-C were synthesized in this study with almost identical molecular weight and polydispersity.

3.4. Fabrication of Polyimide Composite Films Comprising Dual-Porous Silica Nanoparticles. Figure 3 shows the manufacturing procedure of PI/DPS hybrid composite films. The desired content of MPS was adjusted, ranging from 1 to 20 wt % in the aqueous PAA-A and PAA-C solutions. The resulting mixture solutions were cast on a glass plate and dried at 50 °C overnight. The PI/DPS composite films were obtained through a thermal imidization process while raising the temperature to 350 °C stepwise in a vacuum oven. The thickness of the final PI/DPS composite films was controlled to be 80 μm on average with an area of over 10 cm \times 10 cm. Both PI polymers and DPS have excellent thermal stability, so all PI/DPS composite films showed a 5 wt % pyrolysis temperature of 595 °C (Figure S8). Each sample was named PI-X/DPS-# according to the type of PI matrix polymer and the composition by weight of DPS (where X denotes amine (A)- or carboxyl (C)-terminated group). For example, the PI/DPS composite film prepared by hybridizing 5 wt % of DPS with amine-terminated PI is denoted as PI-A/DPS-5. We also note that our procedure for fabricating a composite film is an environmentally sound process releasing water as a major side product.

3.6. Morphologies of PI-A/DPS and PI-C/DPS Composite Films. To confirm the compatibility between the PI matrix and DPS, the surface morphology of each PI/DPS composite film was systematically analyzed through 3D LCM and SEM observations (Figure 4). At first, Figure 4a–d shows the results of LCM observation in the area of 1 mm \times 1.4 mm for the PI-A/DPS-# films with the content of DPS ranging

from 1 to 10 wt %. According to the LCM results, the PI-A/DPS-1 film has a smooth surface (Figure 4a), but in the case of the PI-A/DPS-5 film, some bumps and protruding structures were clearly observed on the surface (Figure 4b). This phenomenon became even more severe as the DPS content increased to 7 and 10 wt %, as shown in Figure 4c,d. The LCM images could quantitatively characterize each sample's surface profile and roughness. As the content of DPS increased from 1 to 10 wt %, the surface roughness (R_a) increased with values of 2.18, 4.62, 20.37, and 25.41 μm for PI-A/DPS-1, PI-A/DPS-5, PI-A/DPS-7, and PI-A/DPS-10 films, respectively. The height of the protruding structure also greatly increased to the value of 10.7, 27.7, 88.8, and 128.8 μm for identical films (Figure S9). The same samples were analyzed with SEM images to confirm the morphology of the surface on a nanometer scale (Figure 4e–h). Even for the PI-A/DPS-1 film, it was observed that DPS are aggregated on the surface throughout the sample. It suggests that the dispersibility of DPS with a highly negative charge deteriorated significantly in the PI-A matrix with cationic end groups. Suppose that such rough composite films are applied to the substrate for practical 5G-communication PCBs. In that case, the interface characteristics with a copper foil are poor, and there is a high possibility of causing serious transmission loss due to the skin effect according to high surface roughness.³⁴

Figure 4i–p shows the LCM and SEM images of the PI-C/DPS-# films. From the LCM images, it can be confirmed that PI-C/DPS-# films show a smoother surface morphology without protruding structures, even when DPS are compounded up to 7 wt %, as shown in Figure 4i–k. In the PI-C/DPS-10 films, agglomerated protrusions at several tens of micrometers were observed. As the DPS content increased from 1 to 10 wt %, the R_a values were 0.77, 2.38, 2.59, and 11.03 μm for PI-C/DPS-1, PI-C/DPS-5, PI-C/DPS-7, and PI-C/DPS-10 films, respectively. It implies that the PI-C/DPS-# films have a remarkably smooth surface morphology compared to the PI-A/DPS-# films (Figure S9). As for the SEM images, the PI-C/DPS-1 and PI-C/DPS-5 films showed a highly smooth surface morphology (Figure 4m,n). However, small granular protrusion structures with a diameter of fewer than 1 μm were observed in the PI-C/DPS-7 film, as shown in Figure 4o. The PI-C/DPS-10 film has a sufficiently smooth surface

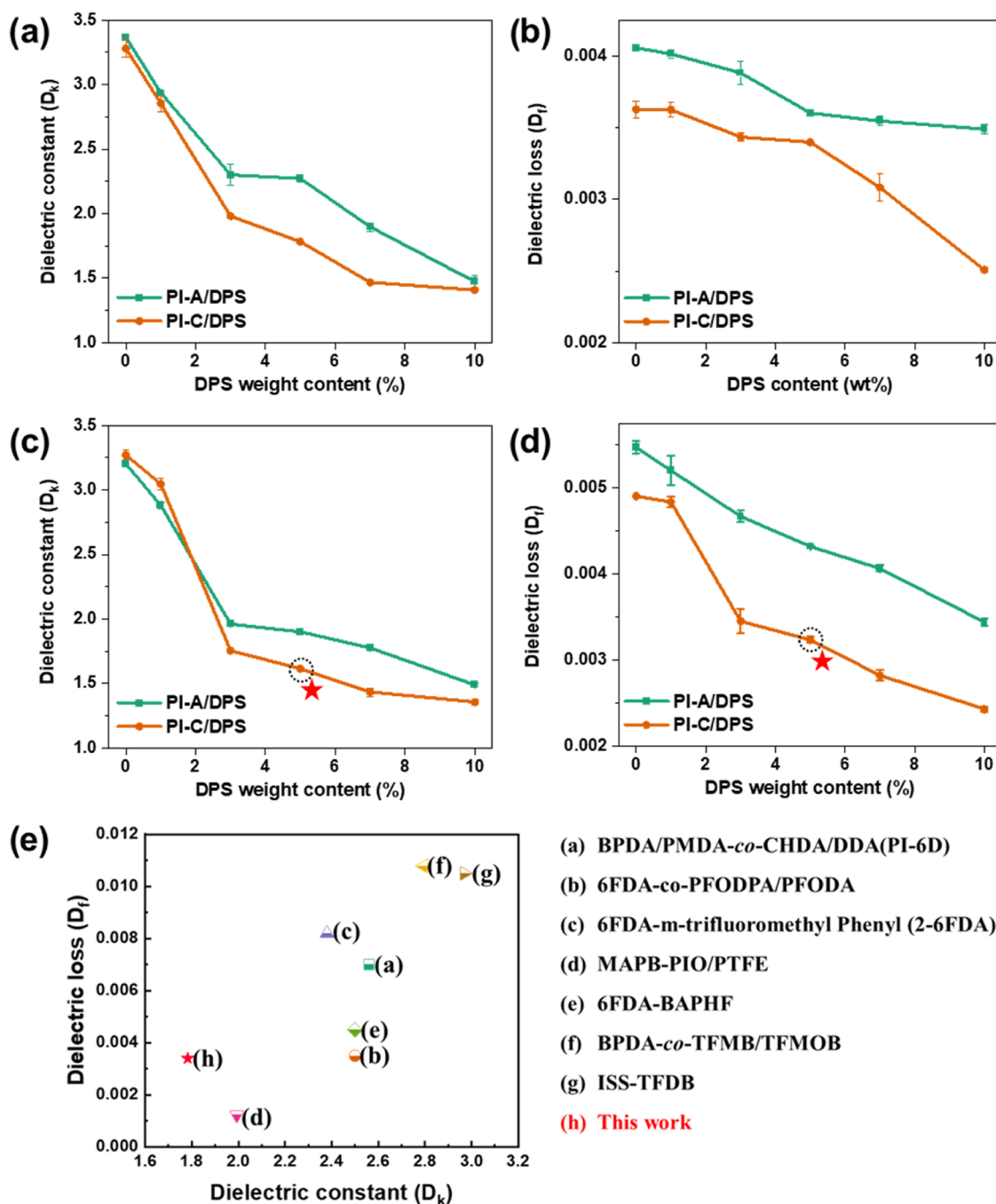


Figure 6. Dielectric properties at (a, b) 10 GHz and (c, d) 28 GHz of PI-A/DPS and PI-C/DPS composite films with various DPS contents. (e) Comparison of the dielectric constant (D_k) and dielectric loss (D_l) at 10 GHz in this work (PI-C/DPS-5) and previous literature.

structure at the micron scale, but the dispersibility of DPS nanofillers can be achieved only when the DPS content is limited below 5 wt %. When the content of DPS nanofillers increases to 10 wt %, it can be seen that more protrusion structures become larger (Figure 4p).

Based on the findings of Figure 4, we discovered that, despite having equal molecular structures and molecular weights, the morphology of the PI-DPS composite film varied significantly depending upon the type of PAA precursor (depending on cationic or anionic end groups). This can be explained by different chemical interactions between MPS and PAA precursors, as shown in Figure 5. The MPS can be dispersed stably in an aqueous medium due to a repulsive force

by the strong surface negative charge. This implies that the electrostatic environment of polymer matrixes can affect the MPS. Distinctively, the PAA-A precursors with cationic end groups anchor the MPS one another, acting as a binder, Figure 5a. Consequently, even at a very low content condition (1 wt %) of MPS, it was possible to observe the aggregated surface morphology easily. As the content of MPS increases, such an interparticular aggregation becomes more severe, and the dimension of the aggregate structure also increases. However, in the case of PAA-C precursors having anionic end groups, the repulsive interactions are predominant between the MPS and the PAA-C precursors so that the dispersibility of MPS can be maintained well (Figure 5b). It makes it possible to fabricate

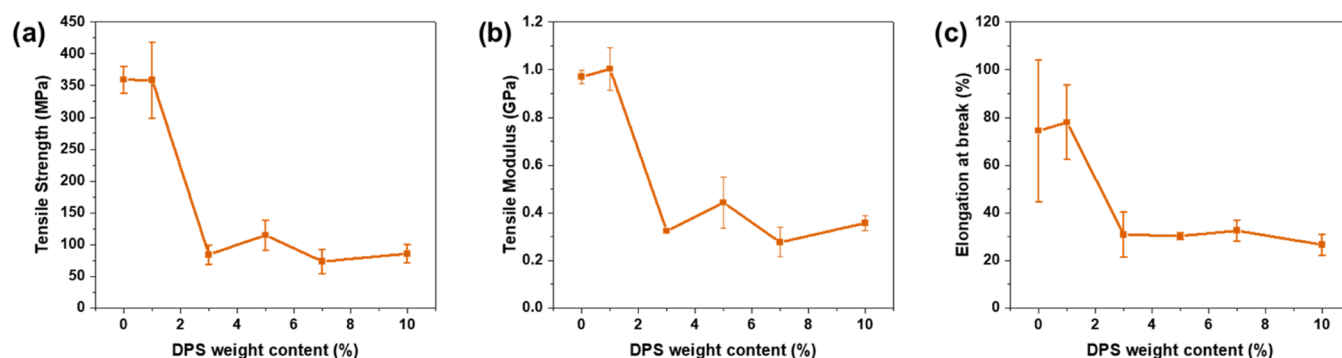


Figure 7. (a) Tensile strength, (b) tensile modulus, and (c) elongation at break of the PI-C/DPS composite films as a function of DPS contents.

Table 1. Mechanical Properties of PI-C/DPS-# Films

	PI-C	PI-C/DPS-1	PI-C/DPS-3	PI-C/DPS-5	PI-C/DPS-7	PI-C/DPS-10
tensile strength (MPa)	359.4 ± 21.14	358.9 ± 59.85	84.3 ± 15.24	114.9 ± 23.29	73.6 ± 18.85	85.6 ± 14.44
tensile modulus (GPa)	0.97 ± 0.03	1.00 ± 0.09	0.32 ± 0.00	0.44 ± 0.11	0.28 ± 0.06	0.36 ± 0.03
elongation at break (%)	74.4 ± 29.64	78.0 ± 15.63	30.9 ± 9.46	30.3 ± 1.41	32.5 ± 4.46	26.6 ± 4.39

highly smooth PI-C/DPS-# composite films, even when the DPS's content increases to 7 wt %.

3.7. Dielectric Properties of PI-A/DPS and PI-C/DPS Composite Films. Figure 6 shows the dielectric properties, D_k and D_f , of PI-A/DPS and PI-C/DPS composite films measured at frequencies of 10 GHz (Figure 6a,b) and 28 GHz (Figure 6c,d). Regardless of the type of PI matrix, D_k decreased as the content of DPS increased, and in particular, when the content of DPS reached the value of over 3 wt %, the values in D_k were reduced significantly at a frequency of 28 GHz (Figure 6a,c). As the DPS content increased from 0 to 10 wt %, the D_k of PI-A/DPS decreased from 3.20 to 1.47, and the D_k of PI-C/DPS decreased from 3.23 to 1.36. This decrease in D_k is due to the increase in air voids ($D_k = 1$) with the introduction of DPS with a hierarchical porous structure. The polarization resulting from the aggregation between DPS can be significantly reduced since DPS are better dispersed in PI-C than in PI-A.

Furthermore, with the introduction of DPS, the chain packing of the BPDA-pPDA polymer backbone was relaxed, resulting in reduced polarization.^{35–37} The decrease in polarization related to dispersibility improvement can be confirmed again through the results for D_f . The D_f of PI-C/DPS-# is much lower than that of PI-A/DPS-# at all DPS contents, both at the measurement frequencies of 10 and 28 GHz, as shown in Figure 6b,d. From the results of the D_f of PI-C–DPS-# measured at 28 GHz, it can be seen that the D_f significantly decreased to less than 0.0035 as the DPS content was over 3 wt %. PI-C/DPS-5 was identified as the most optimal composition considering dispersibility, surface morphology, and dielectric properties. As indicated by a red star in Figure 6c,d, PI-C/DPS-5 showed ultralow dielectric properties with a D_k of 1.615 and a D_f of 0.003 measured at 28 GHz. According to our knowledge, among the PIs or PI-filler composites reported so far, the D_k of the PI-C/DPS developed in this study shows the lowest value measured. Figure 6e shows the comparison of the dielectric properties at 10 GHz in this work (PI-C/DPS-5) with those of other polymeric composite materials reported in the literature (literature values listed in Table S1). Our DPS nanofillers with a hierarchical dual-porous structure can introduce more air voids into the polymer

composite film than the conventional low D_k nanofillers including PTFE, mesoporous silica, and HSP.

3.8. Mechanical Properties of PI-C/DPS Films. The mechanical properties of PI-C/DPS composite films are shown in Figure 7. With increasing contents of DPS, the tensile strength and modulus of the PI-C/DPS composite films gradually decreased (Figure 7a,b). The elongation at break also decreased with the addition of DPS, as shown in Figure 7c. Table 1 summarizes the detailed mechanical properties of PI-C/DPS-# according to the DPS content. Generally, polymer nanocomposites, including inorganic nanofillers, such as ceramic-, metal-, and carbon-based nanoparticles, exhibit improved mechanical properties compared to those neat polymer matrixes.^{38,39} Nevertheless, even though the DPS are evenly distributed and have good compatibility with the PI-C matrix, our results for PI-C/DPS systems contrast with those for traditional PI/inorganic composite systems. The reduction of mechanical properties with the introduction of DPS is attributed to the thin shell of the DPS and the void structure present inside the DPS. Furthermore, the spherical structure of DPS also weakens the mechanical strength of the PI matrix by disturbing the packing of the BPDA-pPDA-based polymer chain. These phenomena can also be confirmed in the results of PI/HSP composite films previously reported by other groups.^{17,40} Nevertheless, our PI-C/DPS-5 composite film identified as the most optimal composition showed a tensile strength of 78.2 MPa, a tensile modulus of 0.32 GPa, and an elongation at break value of 33.9%. It was noted that the PI-C/DPS-5 has mechanical properties applicable to substrates capable of manufacturing flexible electronic devices.⁴¹

4. CONCLUSIONS

We have discussed the preparation and characterization of low dielectric polyimide (PI)/dual-porous silica nanoparticles (DPS) composite films using an eco-friendly aqueous system. A water-based emulsion approach was used to synthesize macroporous silica nanoparticles (MPS) that had been surface-treated with PVP and had outstanding water dispersibility. To test the effective dispersibility with MPS, water-soluble PAAs with various charges at the end group was also “one-step” polymerized in water as the solvent. Both PAAs with positive

and negative charges were prepared by terminating the ends with amine (PAA-A) and carboxyl (PAA-C) groups. The PI/DPS composite films were prepared by hybridizing each PAA and MPS and thermal treatment over 350 °C for an imidization reaction. Furthermore, it was discovered that the MPS were converted into the DPS with macro- and micropore structures during a thermally activated imidization reaction. The dual pore structure of DPS has been identified through the high-resolution TEM and nitrogen adsorption method and significantly contributed to lowering the dielectric constant, D_k , of the PI/DPS composite film. The surface morphology and thermal, dielectric, and mechanical properties of each composite film were observed while controlling the DPS content in the range of 1–10 wt % with a different PI matrix. It was confirmed that PI-C/DPS-5 was the optimal condition considering various properties. The PI-C/DPS-5 composite film with a smooth surface morphology showed ultralow dielectric properties, in which the D_k and D_f were 1.615 and 0.003 at 28 GHz, respectively, and the tensile strength and modulus were 78.2 MPa and 0.32 GPa, respectively. These results can satisfy various physical properties required for substrate materials for 5G communication devices. Our PI/DPS composite film with ultralow D_k and D_f values may be a promising candidate for manufacturing high-frequency communication components such as microantennas in the near future.

■ ASSOCIATED CONTENT

SI Supporting Information

The Supporting Information is available free of charge at <https://pubs.acs.org/doi/10.1021/acsami.2c16197>.

Additional NMR/XPS/FT-IR spectra, SEC trace, TGA thermogram, and optical/LCM images (PDF)

■ AUTHOR INFORMATION

Corresponding Authors

Sunho Jeong – Department of Advanced Materials Engineering for Information and Electronics, Integrated Education Institute for Frontier Science and Technology (BK21 Four), Kyung Hee University, Yongin-si 17104, Korea; Energy Storage Research Center, Korea Institute of Science and Technology, Seoul 02792, Republic of Korea; orcid.org/0000-0002-5969-1614; Email: sjeong@khu.ac.kr

Yun Ho Kim – Advanced Functional Polymers Center, Korea Research Institute of Chemical Technology, Daejeon 34114, Korea; KRICT School, University of Science and Technology, Daejeon 34113, Korea; orcid.org/0000-0002-1722-5623; Email: yunho@kRICT.re.kr

Authors

Sunkyu Kim – Advanced Functional Polymers Center, Korea Research Institute of Chemical Technology, Daejeon 34114, Korea; Department of Chemical Engineering, Hanyang University, Seoul 04763, Korea

Yeongje Lee – Department of Advanced Materials Engineering for Information and Electronics, Integrated Education Institute for Frontier Science and Technology (BK21 Four), Kyung Hee University, Yongin-si 17104, Korea

Jongmin Park – Advanced Functional Polymers Center, Korea Research Institute of Chemical Technology, Daejeon 34114, Korea; orcid.org/0000-0002-9112-6316

Yujin So – Advanced Functional Polymers Center, Korea Research Institute of Chemical Technology, Daejeon 34114, Korea; Department of Chemical and Biomolecular Engineering, Korea Advanced Institute of Science and Technology, Daejeon 34141, Korea

Hee-Tae Jung – Department of Chemical and Biomolecular Engineering, Korea Advanced Institute of Science and Technology, Daejeon 34141, Korea; orcid.org/0000-0002-5727-6732

Min Jae Ko – Department of Chemical Engineering, Hanyang University, Seoul 04763, Korea; orcid.org/0000-0002-4842-3235

Jong Chan Won – Advanced Functional Polymers Center, Korea Research Institute of Chemical Technology, Daejeon 34114, Korea; KRICT School, University of Science and Technology, Daejeon 34113, Korea; orcid.org/0000-0003-3706-7359

Complete contact information is available at:

<https://pubs.acs.org/doi/10.1021/acsami.2c16197>

Author Contributions

[▽]S.K. and Y.L. contributed equally to this work. The manuscript was written with the contributions of all authors. All authors have given approval to the final version of the manuscript.

Notes

The authors declare no competing financial interest.

The authors declare that there is no conflict of interest regarding the publication of this article.

■ ACKNOWLEDGMENTS

This work was supported by KRICT core project (No. SS2221-20), the National Research Foundation of Korea (NRF) grants (NRF-2021M3H4A3A01045740, NRF-2021R1A2C2006771, NRF-2020R1A2C2010067), and the KIST Institutional Program (Project No. 2E31861-22-122).

■ REFERENCES

- (1) Temesvári, Z. M.; Maros, D.; Kádár, P. Review of Mobile Communication and the 5G in Manufacturing. *Proc. Manuf.* **2019**, *32*, 600–612.
- (2) Wang, L.; Yang, J.; Cheng, W.; Zou, J.; Zhao, D. Progress on Polymer Composites With Low Dielectric Constant and Low Dielectric Loss for High-Frequency Signal Transmission. *Front. Mater.* **2021**, *8*, No. 774843.
- (3) Maier, G. Low Dielectric Constant Polymers for Microelectronics. *Prog. Polym. Sci.* **2001**, *26*, 3–65.
- (4) Shamiryan, D.; Abell, T.; Iacopi, F.; Maex, K. Low-k Dielectric Materials. *Mater. Today* **2004**, *7*, 34–39.
- (5) Sroog, C. E. Polyimides. *Prog. Polym. Sci.* **1991**, *16*, 561–694.
- (6) Yang, S.-Y. *Advanced Polyimide Materials: Synthesis, Characterization, and Applications*; Chemical Industry Press, 2018; pp 1–63.
- (7) Ghosh, M. K. *Polyimides: Fundamentals and Applications*; CRC Press, 1996; pp 1–6.
- (8) Zhuang, Y.; Seong, J. G.; Lee, Y. M. Polyimides Containing Aliphatic/Alicyclic Segments in the Main Chains. *Prog. Polym. Sci.* **2019**, *92*, 35–88.
- (9) Kuo, C. C.; Lin, Y. C.; Chen, Y. C.; Wu, P. H.; Ando, S.; Ueda, M.; Chen, W. C. Correlating the Molecular Structure of Polyimides with the Dielectric Constant and Dissipation Factor at a High Frequency of 10 GHz. *ACS Appl. Polym. Mater.* **2021**, *3*, 362–371.
- (10) Liu, Y.; Guo, J.; Wang, J.; Zhu, X.; Qi, D.; Li, W.; Shen, K. A Novel Family of Optically Transparent Fluorinated Hyperbranched

Polyimides with Long Linear Backbones and Bulky Substituents. *Eur. Polym. J.* **2020**, *125*, No. 109526.

(11) Lee, T.; Park, S. S.; Jung, Y.; Han, S.; Han, D.; Kim, I.; Ha, C. S. Preparation and Characterization of Polyimide/Mesoporous Silica Hybrid Nanocomposites Based on Water-Soluble Poly(amic Acid) Ammonium Salt. *Eur. Polym. J.* **2009**, *45*, 19–29.

(12) Han, S.; Li, Y.; Hao, F.; Zhou, H.; Qi, S.; Tian, G.; Wu, D. Ultra-Low Dielectric Constant Polyimides: Combined Efforts of Fluorination and Micro-Branched Crosslink Structure. *Eur. Polym. J.* **2021**, *143*, No. 110206.

(13) Yin, X.; Feng, Y.; Zhao, Q.; Li, Y.; Li, S.; Dong, H.; Hu, W.; Feng, W. Highly Transparent, Strong, and Flexible Fluorographene/Fluorinated Polyimide Nanocomposite Films with Low Dielectric Constant. *J. Mater. Chem. C* **2018**, *6*, 6378–6384.

(14) Yang, K.; Kang, Y. Y.; Ahn, H. J.; Kim, D. G.; Park, N. K.; Choi, S. Q.; Won, J. C.; Kim, Y. H. Porous Boron Nitride/Polyimide Composite Films with High Thermal Diffusivity and Low Dielectric Properties via High Internal Phase Pickering Emulsion Method. *J. Ind. Eng. Chem.* **2020**, *82*, 173–179.

(15) Kourakata, Y.; Onodera, T.; Kasai, H.; Jinnai, H.; Oikawa, H. Ultra-Low Dielectric Properties of Porous Polyimide Thin Films Fabricated by Using the Two Kinds of Templates with Different Particle Sizes. *Polymer* **2021**, *212*, No. 123115.

(16) Chen, Z.; Zhu, D.; Tong, F.; Lu, X.; Lu, Q. Low Dielectric Constant Polyimide Hybrid Films Prepared by in Situ Blow-Balloon Method. *ACS Appl. Polym. Mater.* **2019**, *1*, 2189–2196.

(17) Lee, S. J.; Choi, M. C.; Park, S. S.; Ha, C. S. Synthesis and Characterization of Hybrid Films of Polyimide and Silica Hollow Spheres. *Macromol. Res.* **2011**, *19*, 599–607.

(18) Park, S. S.; Ha, C. S. Polyimide/Hollow Silica Sphere Hybrid Films with Low Dielectric Constant. *Compos. Interfaces* **2016**, *23*, 831–846.

(19) Hong, Z.; Wei, D.; Yong, F.; Hao, C.; Yang, Y.; Yu, J.; Jin, L. Dielectric Properties of Polyimide/SiO₂ Hollow Spheres Composite Films with Ultralow Dielectric Constant. *Mater. Sci. Eng. B* **2016**, *203*, 13–18.

(20) Wang, C.; Wang, Q.; Wang, T. Simple Method for Preparation of Porous Polyimide Film with an Ordered Surface Based on in Situ Self-Assembly of Polyamic Acid and Silica Microspheres. *Langmuir* **2010**, *26*, 18357–18361.

(21) Lee, J.; Park, S. A.; Ryu, S. U.; Chung, D.; Park, T.; Son, S. Y. Green-Solvent-Processable Organic Semiconductors and Future Directions for Advanced Organic Electronics. *J. Mater. Chem. A* **2020**, *8*, 21455–21473.

(22) Cho, K. M.; So, Y.; Choi, S. E.; Kwon, O.; Park, H.; Chan Won, J.; Kim, H.; Jung, H. T.; Kim, Y. H.; Kim, D. W. Highly Conductive Polyimide Nanocomposite Prepared Using a Graphene Oxide Liquid Crystal Scaffold. *Carbon* **2020**, *169*, 155–162.

(23) So, Y.; Bae, H. S.; Kang, Y. Y.; Chung, J. Y.; Park, N. K.; Kim, J.; Jung, H. T.; Won, J. C.; Ryou, M. H.; Kim, Y. H. Eco-Friendly Water-Processable Polyimide Binders with High Adhesion to Silicon Anodes for Lithium-Ion Batteries. *Nanomaterials* **2021**, *11*, No. 3164.

(24) Rahman, I. A.; Padavettan, V. Synthesis of Silica Nanoparticles by Sol-Gel: Size-Dependent Properties, Surface Modification, and Applications in Silica-Polymer Nanocomposites—a Review. *J. Nanomater.* **2012**, *2012*, No. 132424.

(25) Sharma, J.; Polizos, G. Hollow Silica Particles: Recent Progress and Future Perspectives. *Nanomaterials* **2020**, *10*, No. 1599.

(26) Bao, Y.; Wang, T.; Kang, Q.; Shi, C.; Ma, J. Micelle-Template Synthesis of Hollow Silica Spheres for Improving Water Vapor Permeability of Waterborne Polyurethane Membrane. *Sci. Rep.* **2017**, *7*, No. 46638.

(27) Koczur, K. M.; Mourdikoudis, S.; Polavarapu, L.; Skrabalak, S. E. Polyvinylpyrrolidone (PVP) in Nanoparticle Synthesis. *Dalton Trans.* **2015**, *44*, 17883–17905.

(28) Barrett, E. P.; Joyner, L. G.; Halenda, P. P. The Determination of Pore Volume and Area Distributions in Porous Substances. I. Computations from Nitrogen Isotherms. *J. Am. Chem. Soc.* **1951**, *73*, 373–380.

(29) Meškiniš, Š.; Vasilias, A.; Andrulevičius, M.; Peckus, D.; Tamulevičius, S.; Viskontas, K. Diamond like Carbon Films Containing Si: Structure and Nonlinear Optical Properties. *Materials* **2020**, *13*, No. 1003.

(30) Gui-Long, X.; Changyun, D.; Yun, L.; Pi-Hui, P.; Jian, H.; Zhuoru, Y. Preparation and Characterization of Raspberry-like SiO₂ Particles by the Sol-Gel Method. *Nanomater. Nanotechnol.* **2011**, *1*, 79–84.

(31) Keshavarz, H.; Khavandi, A.; Alamolhoda, S.; Naimi-Jamal, M. R. PH-Sensitive Magnetite Mesoporous Silica Nanocomposites for Controlled Drug Delivery and Hyperthermia. *RSC Adv.* **2020**, *10*, 39008–39016.

(32) Martins, T. D.; Ribeiro, T.; Farinha, J. P. S. Overview of Silica-Polymer Nanostructures for Waterborne High-Performance Coatings. *Polymers* **2021**, *13*, No. 1003.

(33) Jeong, Y.; Park, H.; So, Y.; Mun, H. J.; Shin, T. J.; Park, N. K.; Kim, J.; Yoo, S.; Won, J. C.; Kim, Y. H. Enhanced Hydrolytic and Electrical Stability of Eco-Friendly Processed Polyimide Gate Dielectrics for Organic Transistors. *J. Mater. Chem. C* **2020**, *8*, 14370–14377.

(34) Kim, M. K.; Kim, D. W.; Shin, D. W.; Seo, S. J.; Chung, H. K.; Yoo, J. B. A Flexible Insulator of a Hollow SiO₂ Sphere and Polyimide Hybrid for Flexible OLEDs. *Phys. Chem. Chem. Phys.* **2015**, *17*, 2416–2420.

(35) Hardoň, Š.; Kúdelčík, J.; Baran, A.; Michal, O.; Trnka, P.; Hornak, J. Influence of Nanoparticles on the Dielectric Response of a Single Component Resin Based on Polyesterimide. *Polymers* **2022**, *14*, No. 2202.

(36) Zongxiang, W.; Kai, S.; Haikun, W.; Yunpeng, Q.; Jiahong, T.; Licheng, J.; Runhua, F. Epsilon-near-zero response derived from collective oscillation in the metacomposites with ultralow plasma frequency. *Compos. Sci. Technol.* **2022**, *227*, No. 109600.

(37) Zongxiang, W.; Kai, S.; Yunpeng, Q.; Zhongyang, W.; Jiahong, T.; Xiaofeng, L.; Runhua, F. Negative-k and positive-k layers introduced into graphene/polyvinylidene fluoride composites to achieve high-k and low loss. *Mater. Des.* **2021**, *209*, No. 110009.

(38) Tang, B.; Cai, D.; Sun, J.; Wang, J.; Dai, L. Enhanced Mechanical and Thermal Properties of Polyimide/Organically Modified Montmorillonite Hybrid Film Based on Stable Poly (amic Acid) Ammonium Salt. *Polym. Compos.* **2013**, *34*, 2076–2081.

(39) Lin, Y.; Hu, S.; Wu, G. Structure, Dynamics, and Mechanical Properties of Polyimide-Grafted Silica Nanocomposites. *J. Phys. Chem. C* **2019**, *123*, 6616–6626.

(40) Zhang, L.; D'Acunzi, M.; Kappl, M.; Auernhammer, G. K.; Vollmer, D.; Van Kats, C. M.; Van Blaaderen, A. Hollow Silica Spheres: Synthesis and Mechanical Properties. *Langmuir* **2009**, *25*, 2711–2717.

(41) Kim, J.; Kim, B. Y.; Park, S. D.; Seo, J. H.; Lee, C. J.; Yoo, M. J.; Kim, Y. Mechanical Durability of Flexible Printed Circuit Boards Containing Thin Coverlays Fabricated with Poly(amide-imide-urethane)/Epoxy Interpenetrating Networks. *Micromachines* **2021**, *12*, No. 943.